Dense vertical profiling of the natural magnetic field with a suspended QuSpin QTFM Gen 2 under azimuth-balanced acquisition

Andrew Musinov[1]* | Eugene Podgorbuntsev[1] | Roman Gornov[1]

[1] BlueCap Minerals Pty Ltd, Perth, Western Australia, Australia

* Corresponding author: Andrew Musinov · andrew@bluecap.au

ORCID: 0009-0004-0210-5209

Preprint statement
This manuscript is a non-peer-reviewed preprint submitted to EarthArXiv. It has been prepared for subsequent submission to the *Journal of Applied Geophysics*.

Research Paper · Four field sites · 204 processed site-height conditions · 25-50 m sensor AGL

Data and code: Zenodo draft record 22054325 (DOI to be inserted on publication)

Prepared 22 August 2026 · Field experiment conducted 11 March 2026 · Khanh Hoa, Vietnam

Dense vertical profiling of the natural magnetic field with a suspended QuSpin QTFM Gen 2 under azimuth-balanced acquisition

Andrew Musinov[1]*, Eugene Podgorbuntsev[1], Roman Gornov[1]

[1] BlueCap Minerals Pty Ltd, Perth, Western Australia, Australia

* Corresponding author: Andrew Musinov, andrew@bluecap.au

ORCID: https://orcid.org/0009-0004-0210-5209

Highlights

- A suspended QTFM Gen 2 was profiled from 25 to 50 m sensor AGL at 0.5 m intervals.
- Eight to twelve slow yaw turns at each level supported azimuth-balanced field estimates.
- Four natural-field sites produced 204 processed site-height observations.
- The local response near 35 m ranged from -0.7828 to -1.4171 nT/m.
- A physical 34.5-35.5 m acquisition corridor limits the tested pointwise departure to 0.6720 nT.

Abstract

Sensor height is part of the observation geometry of a magnetic survey, yet dense field measurements of installed suspended atomic magnetometers across operational sensor heights remain uncommon. We quantify the pointwise dependence of processed, azimuth-balanced total magnetic field on sensor height above ground level (AGL) for a suspended QuSpin QTFM Gen 2. Experiments were conducted at four agricultural-field sites near Bac Ray Mot and Phuoc Binh, Khanh Hoa, Vietnam. The sensor was carried 20 m below a BlueCapHeli geophysical drone helicopter in a stripped tubular bird. At every nominal level from 25.0 to 50.0 m AGL, separated by 0.5 m, the bird completed 8-12 slow yaw turns. Bird-mounted range LiDAR measured sensor AGL, a matched ground QTFM Gen 2 recorded temporal field variation, acquisition ran at nominal 60 Hz, and wind speed did not exceed 2 m/s. The analytical dataset contains one processed estimate for each of 51 levels at four sites (204 site-height conditions).

Relative to the nominal 35 m value at each site, processed field change at 25 m ranged from +15.8175 to +26.7259 nT and at 50 m from -6.2098 to -10.2615 nT. The complete 25-50 m response span ranged from 22.0273 nT at Site B to 36.9874 nT at Site C. The local gradient near 35 m ranged from -0.7828 to -1.4171 nT/m, while AGL root-mean-square error relative to nominal levels was 0.0792-0.0886 m. Within the full 34.5-35.5 m operational corridor, the maximum absolute pointwise departure from the 35 m reference was 0.6720 nT. The response was systematic but site-specific; the experiment therefore does not support a universal scalar height correction. A normalized inverse-cube series closely matched the processed response (RMSE 0.0429-0.0998 nT), but because that series is a diagnostic benchmark rather than an independent observation, the match is not evidence for a universal inverse-cube law. The results establish a quantitative acquisition and quality-control basis for retaining actual sensor AGL and classifying out-of-corridor data. Spatial continuation equivalence, anomaly broadening, inversion effects and drill-target displacement require a separate experiment using coincident horizontal lines or grids.

Keywords: drone magnetometry; scalar atomic magnetometer; sensor AGL; heading error; harmonic compensation; vertical magnetic-field response; survey quality control

1. Introduction

Small drone-based airborne systems can acquire magnetic data closer to geological sources than conventional crewed surveys. Reduced source-sensor distance increases sensitivity to short-wavelength field components, but also makes the observations more sensitive to sensor trajectory, orientation, platform field and terrain clearance. Observation height is therefore not merely ancillary navigation metadata; it forms part of the survey transfer function.

Increasing sensor height attenuates high spatial frequencies more strongly than low spatial frequencies. Local extrema become smaller and anomalies become broader before levelling, gridding, derivatives or inversion are applied. Field continuation can calculate a magnetic field on a different surface. Upward continuation is generally stable but deliberately smooths the field. Downward continuation attempts to predict a field closer to its sources and amplifies high-frequency measurement noise, geometry error and edge effects unless regularized [8-10,12-14]. Equivalent-source methods can accommodate irregular observation surfaces, but their output remains model-dependent and is not automatically identical to a field physically measured on the target surface [9,14].

This distinction is operationally important for terrain-following drone surveys. A range LiDAR can identify the actual sensor AGL and support quality control and forward modelling. It does not, by itself, demonstrate that data collected over a broad height envelope can be transformed without loss into observations acquired at one physical height. A direct test of that spatial equivalence requires coincident survey lines or grids at multiple heights. The narrower question addressed here is pointwise: how does the processed, azimuth-balanced total-field observation at one horizontal location change as physical sensor AGL changes?

Orientation-dependent error is a second control on mobile atomic magnetometry. An ideal scalar magnetometer reports field magnitude independently of sensor heading, but an installed instrument may retain heading response from optical-pumping physics, nonlinear Zeeman effects, dead-zone geometry, magnetic components of the bird, cables and electronics, and motion. Aeromagnetic compensation and harmonic models are widely used to reduce these effects [2,3,11]. In this experiment, slow repeated yaw turns provided dense azimuthal coverage at every height. Harmonic regression separated the angle-independent intercept used for the height analysis from periodic heading terms.

Temporal geomagnetic variation was monitored with a stationary magnetometer of the same model. Base-station correction is a standard component of aeromagnetic processing [4,5]. A same-model base reduces differences in sensor physics and frequency response, although it does not remove the need to account for inter-instrument offset and the spatial gradient between airborne and ground locations.

The contribution of this work is an installed-system characterization combining four natural-field sites, 51 sensor-height levels per site, repeated full-yaw coverage, direct bird-mounted LiDAR AGL, and a matched ground QTFM. The study tests four hypotheses: (H1) processed azimuth-balanced field changes systematically with sensor AGL; (H2) the magnitude of this change differs among sites; (H3) achieved AGL scatter is substantially smaller than the 0.5 m experimental increment; and (H4) agreement with an inverse-cube benchmark does not establish a universal attenuation law for distributed natural fields.

2. Field setting and operational reference

2.1. Sites

The experiment was conducted on 11 March 2026 at four separate agricultural-field sites near Bac Ray Mot and Phuoc Binh, Xa Bac Ai Tay, Khanh Hoa, Vietnam. Coordinates are WGS 84.

Site	Latitude	Longitude	Decimal degrees	Locality
A	11°59'59.54" N	108°49'00.11" E	11.9998722, 108.8166972	Bac Ray Mot / Phuoc Binh
B	12°00'23.31" N	108°49'07.11" E	12.0064750, 108.8186417	Bac Ray Mot / Phuoc Binh
C	12°00'46.07" N	108°49'15.44" E	12.0127972, 108.8209556	Bac Ray Mot
D	12°00'58.49" N	108°48'51.74" E	12.0162472, 108.8143722	Bac Ray Mot / Phuoc Binh

The sites were open fields away from buildings and without a deliberately emplaced magnetic target. A known artificial source was unnecessary because the objective was to characterize the installed system in the spatially varying natural field encountered during survey operations. This condition does not imply the absence of geological sources or local crustal gradients.

2.2. Weather and reference height

Flights were scheduled for calm conditions. Wind was measured with a Kestrel 5500 with LiNK and did not exceed 2 m/s during the four experiments. Low wind reduced irregular pendulum motion and supported slow free yaw rotation.

BlueCap uses 35 m sensor AGL as a lower operational and safety reference for the class of valley surveys considered here, where trees and isolated canopy or obstacle features can rise above surrounding terrain. The complete one-metre experimental compliance corridor is 34.5-35.5 m. Higher sensor AGL may be required for obstacle clearance and remains valid as a different observation geometry. The 35 m value is an operational rule for this survey context, not a universal safe height for all terrain, vegetation or aviation conditions.

3. Instrumentation

3.1. Airborne magnetometer and suspended bird

The airborne sensor was a QuSpin QTFM Gen 2 scalar total-field atomic magnetometer installed in a BlueCapBird. The aerodynamic wings were removed for the experiment, leaving a predominantly tubular body that could rotate about the near-vertical suspension axis. The bird was connected to the BlueCapHeli by a pre-measured 20 m line.

The scalar zero-crossing count was set to SZC/ZC = 100. QuSpin identifies this as the Average magnetic-environment profile, intermediate between Noisy = 40 and Quiet = 200. A larger zero-crossing count favours sensitivity in a quiet field, whereas a smaller value increases tolerance to magnetic noise and motion [16,17]. All programmable onboard digital filters were Off. Thus the QTFM 50/60 Hz notch and programmable low-pass, high-pass and custom filters did not shape the acquired output [18]. Downstream condition averaging is distinct from these onboard filters.

Published manufacturer specifications give typical QTFM Gen 2 scalar sensitivity of approximately 3 pT/sqrt(Hz) and uncompensated heading error below 3 nT [1]. These standalone specifications do not represent installed survey noise and are not outcomes of the present condition-level analysis.

3.2. Carrier, positioning and height channels

BlueCapHeli is a 25 kg-class single-rotor petrol drone helicopter developed and operated as a carrier for magnetic, LiDAR, radiometric and imaging surveys [15]. Helicopter height was controlled using BlueCapRTK. A nominal height condition was accepted only after a stable RTK fixed solution and a reported vertical solution accuracy of 0.005 m were achieved. This threshold describes the navigation acceptance criterion for the carrier; it is not a claim of 5 mm absolute position accuracy for the suspended QTFM.

Sensor position was constrained by synchronized bird GNSS, IMU/heading and range-LiDAR channels together with the known suspension length, carrier RTK trajectory, wind and an aerodynamic-pendulum model. In an operational reconstruction, these measurements can be fused by a constrained nonlinear state estimator, such as an extended or unscented Kalman filter followed by Rauch-Tung-Striebel smoothing, or by factor-graph optimization. The bird GNSS directly limits accumulated model drift, the carrier RTK constrains the suspension point, and LiDAR independently constrains sensor height above the local surface.

The range LiDAR was mounted on the bird and measured distance to the surface. Actual sensor AGL was obtained from LiDAR with the recorded attitude and surface geometry. The achieved condition-level AGL statistics reported below are derived from the processed workbook and supersede any assumption that carrier RTK accuracy alone describes sensor height accuracy.

3.3. Ground magnetic reference

A second QTFM Gen 2 was installed on the ground approximately 35 m horizontally from the projection of the suspended sensor. It continuously monitored temporal magnetic-field variation during each flight. Correction used the temporal departure of the base record from a selected reference epoch rather than subtracting its entire absolute level, which would mix diurnal variation with local gradient, height difference and inter-instrument offset.

4. Experimental procedure

At take-off, an initial yaw impulse was applied to the stripped tubular bird. The bird then rotated freely. The helicopter increased height sequentially while the bird-mounted LiDAR monitored sensor AGL. Only an ascending order was used.

Each site followed the same nominal program:

1. start at 25.0 m sensor AGL;
2. acquire at 0.5 m increments;
3. finish at 50.0 m sensor AGL;
4. retain 8-12 complete slow yaw turns at each level; and

5 record QTFM and synchronized instrumentation at a nominal 60 Hz.

The complete sequence contains 51 nominal height conditions per site and approximately 408-612 rotations per flight. Across four sites this corresponds to 204 site-height conditions and approximately 1632-2448 rotations. Individual rotations are acquisition controls, not independent statistical replicates in this paper. Each flight lasted approximately 95-105 min.

Because all levels were acquired upward, height is correlated with elapsed time, fuel or power state, electronic temperature and possible changes in yaw rate. The simultaneous base station constrains temporal geomagnetic variation but cannot remove every time-height confounder. A repeated experiment should randomize, descend, or otherwise balance height order.

5. Processing and analysis

5.1. Synchronization and temporal correction

Instrument channels were placed on a common UTC timeline while retaining native timestamps. Time offsets and drift must be evaluated independently of magnetic-residual minimization to avoid circular alignment. A temporal correction can be written as

$$T_{dc}(t) = T_{air}(t) - [T_{base}(t) - T_{base}(t_{ref})],$$

where T_{air} is airborne total field, T_{base} is ground total field, and t_{ref} defines the retained reference level. Base records were screened conceptually for spikes, dropouts, timing consistency, platform influence, orientation stability and local-gradient effects before correction.

5.2. Height conditions and azimuth-balanced estimates

Height plateaus were identified from LiDAR AGL and event or flight channels. Actual height statistics were associated with each nominal level. Yaw was unwrapped to identify complete rotations, and transition segments between levels were excluded from the condition estimates.

At site s and height h, the corrected magnetic record was represented by a harmonic nuisance model:

$$T_{dc,s,h}(t) = \beta_{0,s,h} + \sum_{k=1}^{K} \{a_{k,s,h} \cos[k\,\psi(t)] + b_{k,s,h} \sin[k\,\psi(t)]\} + \epsilon(t),$$

where β_0 is the azimuth-balanced total-field estimate, a_k and b_k are periodic heading coefficients, ψ is yaw, K is a preselected model order, and ϵ includes remaining noise, motion effects and autocorrelation. The amplitude of harmonic k is $A_k = \sqrt{a_k^2 + b_k^2}$. The public condition-level dataset contains β_0-type processed means, not individual 60 Hz samples or harmonic coefficients.

5.3. Height-response quantities

For each site, pointwise height response was expressed relative to the nominal 35 m condition:

$$\Delta T_s(h) = \beta_{0,s}(h) - \beta_{0,s}(35\ \mathrm{m}).$$

The local gradient near 35 m was calculated by a central difference between the nominal 34.5 and 35.5 m conditions using their measured AGL values. Additional metrics were AGL RMSE relative to nominal levels, complete 25-50 m response span, and RMSE between the processed anomaly and a normalized $1/r^3$ diagnostic series.

The inverse-cube series is a benchmark anchored to the site-specific value at 35 m. It represents a compact-source far-field form and is not imposed as a physical law for the distributed natural field. Because it is calculated rather than independently measured, close agreement cannot validate a universal attenuation model.

The unit of analysis is the processed site-height condition ($n = 204$). Raw 60 Hz noise, individual-turn repeatability, harmonic uncertainty, invalid/dead-zone fraction, spatial spectra and crossover statistics are outside the released dataset and are not inferred from the smooth condition-level curves.

6. Results

6.1. Experimental coverage and regional field context

All four sites contain 51 processed nominal height conditions from 25 to 50 m AGL. NOAA WMMHR2025 gives a modelled total main or regional field near 35 m on 11 March 2026 of approximately 41,917.0 nT at Site A, 41,918.3 nT at Site B, 41,919.2 nT at Site C and 41,919.4 nT at Site D [7]. The WMM uncertainty in F is approximately 134 nT, and the predicted change over 25-50 m is only about -0.6 nT at Site A. WMM represents the large-scale field and does not predict local crustal structure or the observed temporal field.

6.2. Processed pointwise height response

The processed field decreased with increasing height at all four sites, but its magnitude and local gradient differed (Table 1; Figure 1). At 25 m, Delta T was +15.8175 to +26.7259 nT. At 50 m, Delta T was -6.2098 to -10.2615 nT. The smallest complete response span was 22.0273 nT at Site B and the largest was 36.9874 nT at Site C.

Table 1. Site-level processed height-response metrics.

Site	T_mean at 35 m (nT)	Delta T at 25 m (nT)	Delta T at 50 m (nT)	dT/dh near 35 m (nT/m)	AGL RMSE (m)	Response span (nT)	RMSE vs 1/r^3 (nT)
A	41,923.9551	+21.3432	-8.1743	-1.2091	0.0804	29.5175	0.0448
B	41,931.2545	+15.8175	-6.2098	-0.7828	0.0792	22.0273	0.0523
C	41,926.1837	+26.7259	-10.2615	-1.4171	0.0804	36.9874	0.0998
D	41,937.4236	+19.2694	-7.6459	-0.9152	0.0886	26.9153	0.0429

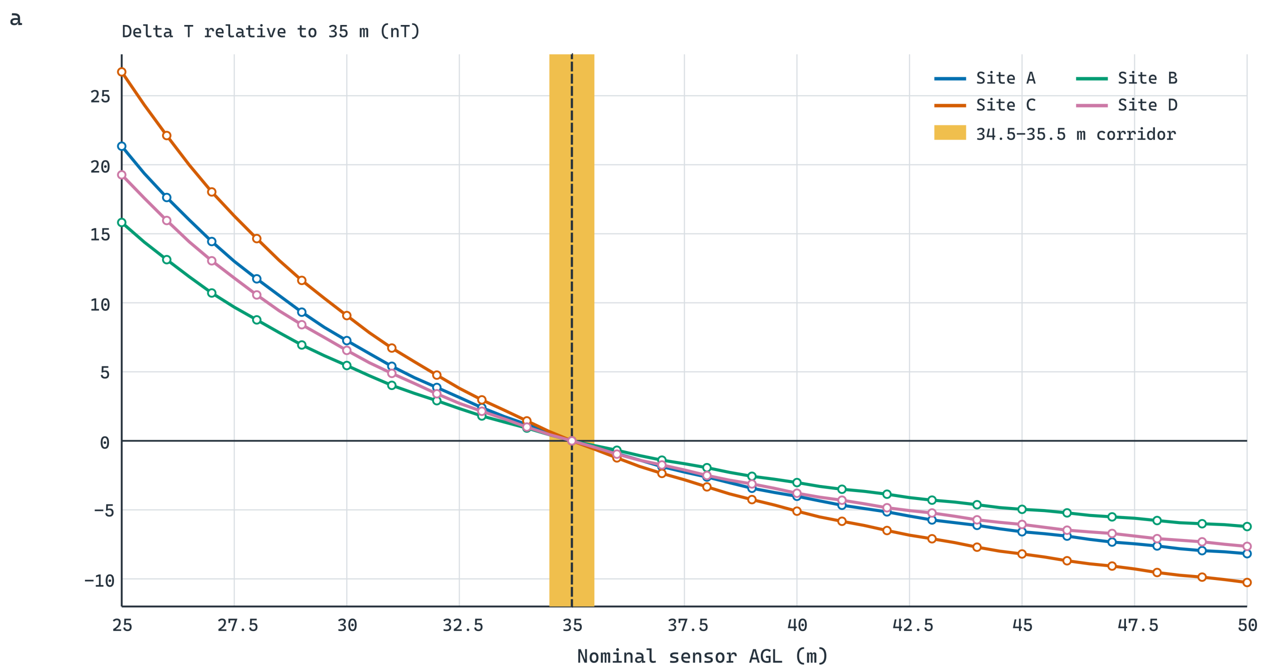

Figure 1. Processed pointwise height response at four sites. Delta T is referenced independently to the nominal 35 m condition at each site. The gold band marks the full 34.5-35.5 m operational corridor. Each curve contains 51 condition-level observations at 0.5 m nominal spacing.

Site dependence is evident in both range and slope. The magnitude of the local gradient differs by a factor of approximately 1.8 between Sites B and C. A single site-independent scalar correction is therefore not supported by these observations.

6.3. Operational corridor

At the nominal 34.5 m conditions, Delta T ranged from +0.4403 to +0.6720 nT; at 35.5 m it ranged from -0.3425 to -0.6034 nT. Thus, the largest absolute pointwise departure at the boundaries of the tested one-metre corridor was 0.6720 nT. A 1 m departure near 35 m corresponds locally to approximately 0.8-1.4 nT, while larger departures become increasingly nonlinear. At 30 m, Delta T was +5.4560 to +9.0737 nT; at 40 m it was -3.0232 to -5.0946 nT.

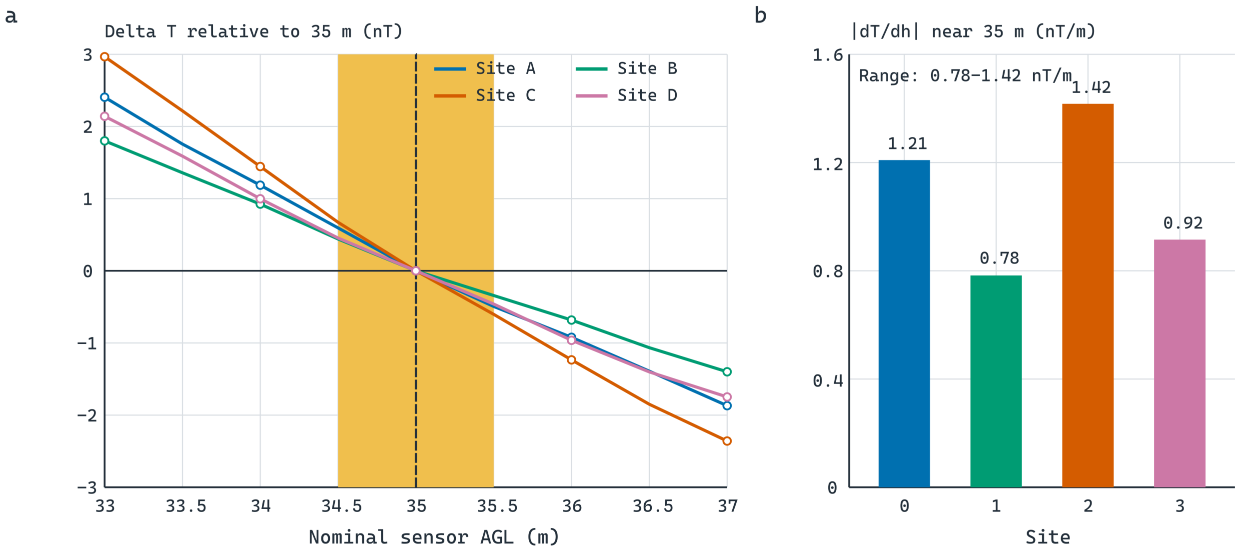

Figure 2. (a) Processed response from 33 to 37 m with the complete 34.5-35.5 m corridor highlighted. (b) Absolute local gradient calculated by central difference between measured AGL at the nominal 34.5 and 35.5 m levels.

Achieved AGL RMSE relative to nominal height was 0.0792-0.0886 m. These observed values are larger than a centimetre-scale assumption and should be used when describing the geometry of the condition-level data.

6.4. Inverse-cube diagnostic

The normalized 1/r^3 benchmark matched the processed response with site-level RMSE of 0.0429-0.0998 nT (Figure 3). Such close agreement is reported transparently but interpreted conservatively. The predicted series was generated from the workbook model and anchored to site-specific response; it is not a second instrument record or a blind prediction. Consequently, the result is a model-diagnostic observation, not independent proof that the distributed natural field follows a universal inverse-cube law.

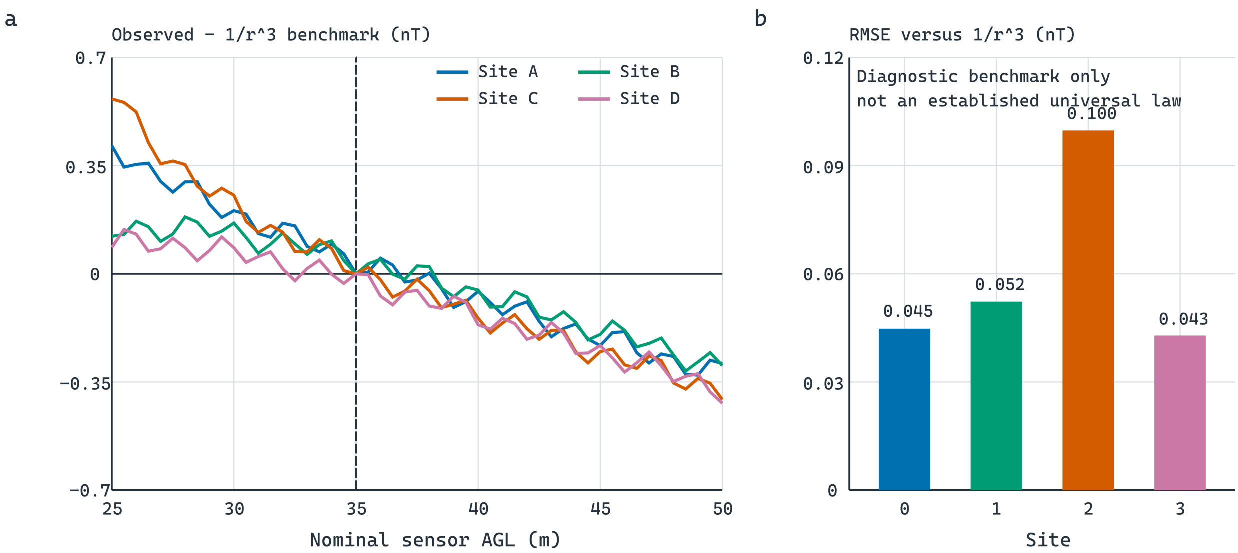

Figure 3. (a) Residual between observed processed response and the normalized nominal-height 1/r^3 benchmark. (b) Site-level benchmark RMSE. The benchmark is not an independent observation.

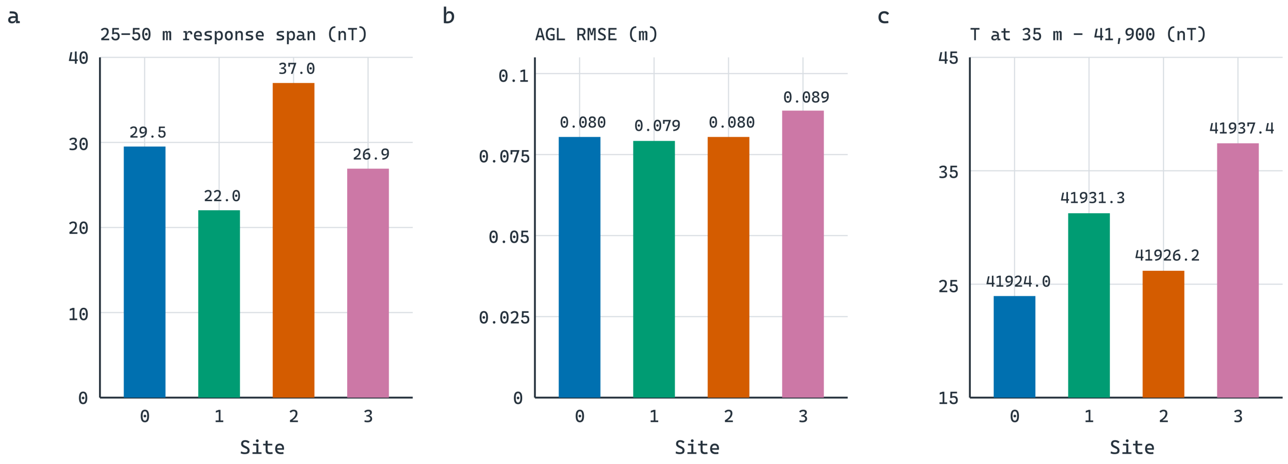

Figure 4. Site-level summary of complete response span, local gradient magnitude near 35 m, achieved AGL RMSE and inverse-cube benchmark RMSE.

7. Discussion

7.1. What the experiment establishes

The four vertical profiles establish a repeatable pointwise relationship between physical sensor AGL and the processed azimuth-balanced field of the installed QTFM Gen 2 system. All sites show the same direction of change across the tested interval, yet response magnitude differs materially. The result supports H1-H3: height response is systematic, site-specific, and resolved with achieved AGL error well below the 0.5 m experimental increment.

The experiment also shows why sensor AGL should remain attached to every accepted magnetic observation. A height excursion can produce a field change before any geological processing begins. If geometry changes are not retained and classified, they can be interpreted silently as spatial geology during levelling, gridding or inversion.

For client-facing quality control, three acquisition states should be distinguished:

1. **Compliant acquisition:** actual sensor AGL lies within 34.5-35.5 m.
2. **Deliberately higher acquisition:** height is increased for safety or obstacle clearance and retained as a different observation geometry.
3. **Unplanned excursion:** departure from the target corridor is recorded by LiDAR and reviewed for acceptance, re-flight or interpretation impact.

An out-of-corridor observation is not automatically unusable. Its comparability depends more strongly on local geology, trajectory quality and the assumptions of subsequent height modelling. The experiment does not support replacing physical height control with one universal Delta T-per-metre correction.

7.2. Interpretation boundary

Vertical hover profiles measure how one point observation changes with height. They do not measure lateral anomaly broadening, attenuation of individual wavenumbers along a line, or equivalence between a continued field and a physical observation on the target surface. Those claims require coincident horizontal lines or grids acquired physically at multiple sensor heights. A continuation study should compare real 25 or 30 m lines upward-continued to 35 m, and real 40, 45 or 50 m lines downward-continued to 35 m, against a physically acquired 34.5-35.5 m reference.

For the same reason, the present study does not quantify a displacement in a 2D map, 3D inversion or drill target. It establishes the first causal link: AGL departure changes the processed magnetic observation. Downstream effects on anomaly geometry, inferred source depth or planned drill intercept require the spatial experiment.

7.3. Installed noise and comparison with other sensors

Smooth condition means are not measurements of intrinsic noise floor or installed survey noise. This dataset cannot yield amplitude spectral density, fourth-difference noise, raw standard deviation, turn-to-turn repeatability, line-to-line noise or residual heading error. It therefore does not demonstrate that QTFM Gen 2 is quieter than Geometrics MagArrow II.

Manufacturer specifications provide context only. QTFM Gen 2 lists typical scalar sensitivity near 3 pT/sqrt(Hz) and uncompensated heading error below 3 nT [1], whereas the MagArrow II sheet lists typical noise or sensitivity of 5 pT/sqrt(Hz) and typical heading error of +/-5 nT over a full rotation [19]. The values arise from different instruments, procedures and bandwidth conventions. A defensible comparison requires coincident lines, common bandwidth and timing, the same physical AGL, PSD or ASD, fourth differences, crossover statistics and blind comparison of final maps.

The installed configuration has explicit trade-offs. SZC/ZC = 100 favours robustness over the maximum quiet-field sensitivity of SZC = 200. Filters Off preserves broadband output and avoids onboard phase or amplitude shaping, but leaves mains, platform and high-frequency components for downstream treatment. The 20 m suspension reduces carrier magnetic influence while increasing the need for trajectory reconstruction and pendulum control. Ascending-only acquisition does not test order hysteresis.

8. Conclusions

1 Four sites and 51 heights per site produced 204 processed conditions. Relative to 35 m, Delta T was +15.8175 to +26.7259 nT at 25 m and -6.2098 to -10.2615 nT at 50 m.

2 Pointwise height response was site-specific. Complete span ranged from 22.0273 to 36.9874 nT, and the local gradient near 35 m ranged from -0.7828 to -1.4171 nT/m.

3 AGL RMSE relative to nominal levels was 0.0792-0.0886 m and should be used in preference to a centimetre-scale assumption for this dataset.

4 Within 34.5-35.5 m, the largest tested absolute pointwise departure from nominal 35 m was 0.6720 nT. Higher acquisition remains permissible for safety but constitutes a different observation geometry.

5 The inverse-cube benchmark RMSE of 0.0429-0.0998 nT is diagnostic only because the predicted series is model-generated and anchored, not independently observed.

6 The evidence supports continuous actual-sensor-AGL recording, corridor-compliance classification and field review of excursions. It does not quantify spatial continuation error, inversion error or drill-target displacement.

CRediT authorship contribution statement

Andrew Musinov: Conceptualization, Methodology, Investigation, Resources, Project administration, Supervision, Writing - original draft, Writing - review and editing. Eugene Podgorbuntsev: Methodology, Formal analysis, Data curation, Validation, Visualization, Writing - review and editing. Roman Gornov: Investigation, Validation, Resources, Writing - review and editing.

Funding

This research received no external funding and was supported internally by BlueCap Minerals Pty Ltd.

Declaration of competing interest

All authors are affiliated with BlueCap Minerals Pty Ltd. Andrew Musinov is the company's Managing Director. BlueCap Minerals Pty Ltd develops and operates the BlueCapHeli and BlueCapBird systems discussed in this study and therefore has a commercial interest in the operational application of the reported results.

Data and code availability

The curated processed data, site coordinates, metadata and figure-generation code supporting this study are held in private Zenodo draft record 22054325 and will be released when the record is published. The final manuscript will cite the registered Zenodo DOI. Proprietary control implementations and restricted commercial information are excluded from the public package; the repository README documents this boundary. The public analytical unit is the processed site-height condition, not the raw 60 Hz, individual-turn, IMU or base-station time series.

Declaration of generative AI and AI-assisted technologies

OpenAI Codex was used solely to assist with manuscript structuring. The authors reviewed the final manuscript and take full responsibility for its content.

Acknowledgements

The authors thank the BlueCap field operations and data engineering personnel who supported equipment preparation and the Vietnam field programme.

References

1. QuSpin. QTFM Gen 2 Scalar Total-Field Atomic Magnetometer. https://quspin.com/qtfm-gen-2/.

2. Phelps, G., Bracken, R., Spritzer, J., White, D. (2022). Achieving sub-nanoTesla precision in multirotor UAV aeromagnetic surveys. *Journal of Applied Geophysics*, 206, 104779. https://doi.org/10.1016/j.jappgeo.2022.104779.

3. Liu et al. (2020). Aeromagnetic compensation with suppressing heading error of the scalar atomic magnetometer. *IEEE Geoscience and Remote Sensing Letters*. https://doi.org/10.1109/LGRS.2019.2940824.

4. White, D.J. et al. (2015). Levelling aeromagnetic survey data without the need for tie-lines. *Geophysical Prospecting*. https://doi.org/10.1111/1365-2478.12198.

5. Zhang et al. (2023). Development of a hybrid fixed-wing UAV aeromagnetic survey system and an application study in Chating Deposit. *Minerals*, 13(8), 1094. https://doi.org/10.3390/min13081094.

6. U.S. Geological Survey (2026). High-resolution magnetic survey using an unoccupied aerial vehicle to constrain buried lava flow geometry, volume, and eruptive history of Little Cones, Crater Flat, Nevada. https://pubs.usgs.gov/publication/pp1890R/full.

7. NOAA NCEI Geomagnetic Modeling Team and British Geological Survey (2024). World Magnetic Model 2025. https://www.ncei.noaa.gov/products/world-magnetic-model.

8. Ekinci, Y.L. (2021). On the drape and level flying aeromagnetic survey modes with terrain effects, and data reduction between arbitrary surfaces. *Turkish Journal of Earth Sciences*, 30(3), 409-424. https://doi.org/10.3906/yer-2007-18.

9. Gavazzi, B. et al. (2020). On the use of aeromagnetism for geological interpretation: comparison of scalar and vector magnetometers and an equivalent source interpolator for fixed-altitude and draping data sets. *Journal of Geophysical Research: Solid Earth*, 125. https://doi.org/10.1029/2019JB018870.

10. Gang, Y., Zhang, L. (2018). An improved stable downward continuation of potential fields using a truncated Taylor series and regularized vertical derivatives method. *Journal of Geophysics and Engineering*, 15(5), 2001-2008. https://doi.org/10.1088/1742-2140/aac53a.

11. Kaub, L., Keller, G., Bouligand, C., Glen, J.M.G. (2021). Magnetic surveys with unmanned aerial systems: software for assessing and comparing the accuracy of different sensor systems, suspension designs and compensation methods. *Geochemistry, Geophysics, Geosystems*, 22, e2021GC009745. https://doi.org/10.1029/2021GC009745.

12. Pilkington, M., Roest, W.R. (1992). Draping aeromagnetic data in areas of rugged topography. *Journal of Applied Geophysics*, 29(2), 135-142. https://doi.org/10.1016/0926-9851(92)90004-5.

13. Cooper, G.R.J. (2004). The stable downward continuation of potential field data. *Exploration Geophysics*, 35(4), 260-265. https://doi.org/10.1071/EG04260.

14. Zuo, B. et al. (2020). Downward continuation and transformation of total-field magnetic anomalies into magnetic gradient tensors between arbitrary surfaces using multilayer equivalent sources. *Geophysical Research Letters*. https://doi.org/10.1029/2020GL088678.

15. BlueCap (2026). BlueCapHeli - long-endurance petrol drone helicopter for geophysical surveys. https://bluecap.au/survey-equipment/bluecapheli-gasoline-helicopters-long-endurance-australia/.

16. QuSpin (2026). QTFM Gen 2 Sensor Configuration. https://quspin.com/qtfm-gen-2/qtfm-gen-2-user-guide/sensor-configuration/.

17. QuSpin (2026). QTFM Gen 2 Configuration Profiles. https://quspin.com/qtfm-gen-2/qtfm-gen-2-user-guide/qtfm2-sensor-profile-configuration/.

18. QuSpin (2026). QTFM Gen 2 Quick Reference: Serial Commands and Filters. https://quspin.com/qtfm-gen-2-quick-reference/.

19. Geometrics (2023). MagArrow II Drone-Deployable Magnetometer - Specifications. https://www.geometrics.com/wp-content/uploads/2023/08/MagArrow_II_UAS_SpecSheet_07212023.pdf.